

#### Contents lists available at ScienceDirect

# Petroleum Science

journal homepage: www.keaipublishing.com/en/journals/petroleum-science



# Original Paper

# Development and evaluation of organic/metal ion double crosslinking polymer gel for anti-CO<sub>2</sub> gas channeling in high temperature and low permeability reservoirs



Hong-Bin Yang <sup>a, b, \*</sup>, Hai-Zhuang Jiang <sup>a, b</sup>, Zhe Xu <sup>c</sup>, Xing Zhang <sup>d</sup>, Tao Wang <sup>d</sup>, Hai-Ning Liu <sup>e</sup>, Xiao Ma <sup>e</sup>, Jian-Jun Zhu <sup>e</sup>, Xiang-Feng Zhang <sup>d</sup>, Wan-Li Kang <sup>b</sup>

- <sup>a</sup> State Key Laboratory of Deep Oil and Gas, China University of Petroleum (East China), Qingdao, 266580, Shandong, China
- <sup>b</sup> School of Petroleum Engineering, China University of Petroleum (East China), Qingdao, 266580, Shandong, China
- <sup>c</sup> Jianghan Oilfield of Sinopec, Qianjiang, 433124, Hubei, China
- <sup>d</sup> Petroleum Engineering Technology Research Institute, Shengli Oilfield Branch of Sinopec, Dongying, 257000, Shandong, China
- e Dongsheng Jinggong Petroleum Development Group Co., Ltd, Shengli Oilfield Branch of Sinopec, Dongying, 257000, Shandong, China

#### ARTICLE INFO

# Article history: Received 4 August 2024 Received in revised form 25 November 2024 Accepted 25 November 2024 Available online 27 November 2024

Edited by Yan-Hua Sun

Keywords: High temperature and low permeability reservoir CO<sub>2</sub> flooding Anti-gas channeling Polymer gel

#### ABSTRACT

CO<sub>2</sub> flooding enhanced oil recovery (CO<sub>2</sub>-EOR) represents a significant technology in the low permeability reservoir. With the fractures and heterogeneity in low permeability reservoirs, CO2-EOR is susceptible to pessimistic gas channeling. Consequently, there is a need to develop conformance control materials that can be used in CO2-EOR. Herein, to address the challenges of low strength and poor stability of polymer gel in high temperature and low permeability reservoirs, a new organic/metal ion composite crosslinking polymer gel (AR-Gel) is reported, which is formed by low hydrolysis and medium to high molecular weight polymer (CX-305), organic crosslinking agent (phenolic resin), and aluminium citrate (Al(III)). The crosslinking of Al(III) with carboxyl group and organic/metal ion double crosslinking can construct a more complex and stable polymer gel structure on the basis of traditional chemical crosslinking, to cope with the harsh conditions such as high temperature. The structure-activity relationship of AR-Gel was revealed by rheology behavior and micro-morphology. The applicability of AR-Gel in reservoir was investigated, as was its strength and stability in supercritical CO2. The anti-gas channeling and enhanced oil recovery of AR-Gel were investigated using low permeability fractured cores, and the field process parameters were provided. The gel can be used to meet supercritical CO<sub>2</sub> reservoirs at 110 °C and 20,000 mg/L salinity, with long-term stability over 60 days. The plugging rate of AR-Gel for fractured core was 97%, with subsequent CO<sub>2</sub> flooding resulting in an enhanced oil recovery by 34.5%. AR-Gel can effectively control CO2 gas channeling and enhanced oil recovery. It offers a new material with high strength and temperature resistance, which is particularly beneficial in the CO2 flooding for the conformance control of oil field.

© 2024 The Authors. Publishing services by Elsevier B.V. on behalf of KeAi Communications Co. Ltd. This is an open access article under the CC BY-NC-ND license (http://creativecommons.org/licenses/by-nc-nd/4.0/).

#### 1. Introduction

Carbon dioxide (CO<sub>2</sub>) is readily soluble in crude oil due to its similar polarity. This property can enhance the recovery rate of crude oil through dissolution, viscosity reduction, and expansion (Dogah et al., 2021; Jiang et al., 2024; Kang et al., 2021). CO<sub>2</sub> enhanced oil recovery (CO<sub>2</sub>-EOR) technology not only increases

\* Corresponding author. E-mail address: hongbinyang@upc.edu.cn (H.-B. Yang). crude oil production, but also sequesters CO<sub>2</sub> in the original storage space, thereby achieving carbon sequestration (Jiang et al., 2021; Ren and Duncan, 2019; Sharma et al., 2022; Yang et al., 2023). In low permeability reservoirs, CO<sub>2</sub>-EOR is demonstrably more advantageous than water flooding (Cui et al., 2022; Wang et al., 2014; Yang et al., 2024). The use of CO<sub>2</sub> for oil drive in low-permeability oilfields is becoming increasingly prevalent, in line with the global environmental governance initiative and the advancement of carbon capture, utilization and storage (CCUS) technology (Liu et al., 2022). Kumar et al. (2022) conducted a comprehensive analysis of the advantages, mechanisms, and potential drawbacks

of using CO<sub>2</sub> for oil recovery. Their findings suggest that CO<sub>2</sub> will likely become a ubiquitous component of oilfield production enhancement measures. Davoodi et al. (2024) presented recommendations for the implementation and operation of CO<sub>2</sub>-EOR projects in a more efficient manner, as well as how to strategy on the potential opportunities and overcoming the challenges associated with such projects. Nevertheless, in low-permeability oilfields where there are advantageous seepage channels, such as fractures, developed by hydraulic fracturing, CO<sub>2</sub> will finger along fractures with high permeability, resulting in serious gas channeling (Zhou et al., 2021, 2022). CO<sub>2</sub> gas channeling in oilfields can be likened to the phenomenon of "arterial bleeding" in humans, whereby leads to ineffective CO2 circulation, lower crude oil production, and poor carbon sequestration efficiency. Therefore, the anti-CO<sub>2</sub> gas channeling in oilfields is a special concern for CO<sub>2</sub>-EOR (Hao et al., 2016).

A plethora of chemical method anti-CO<sub>2</sub> gas channeling techniques has been developed by petroleum scholars through a combination of laboratory experiments and field applications (Gandomkar et al., 2021; Kang et al., 2019; Pal et al., 2022; Tang et al., 2020). Massarweh and Abushaikha (2022) provided a comprehensive overview of the various techniques employed for anti-CO2 gas channeling, including CO2 water alternating gas injection (CO2-WAG), polymer-assisted CO2 injection, surfactantassisted CO2 mobility control (CO2 foam), and nanoparticleassisted CO2 flooding. The study indicated that each of the aforementioned methods was capable of addressing multiple problems associated to conventional CO2 flooding to some extent. Polymer gel is high-strength material that is capable of long-term stabilization in strata and has recently attracted considerable attention. Ding et al. (2023) reviewed advances in CO<sub>2</sub>-responsive gels, where CO<sub>2</sub> acts as a switch to transform low-viscosity liquids into highviscosity gels, and discussed future directions for such gel systems to focus on. Jansen-van Vuuren et al. (2023) reviewed the development potential of CO<sub>2</sub>-responsive gels for CO<sub>2</sub>-EOR and carbon sequestration. Brattekås and Seright (2023) summarized the application of polymer gels for the conformance control of CO<sub>2</sub> in the oilfield field. The study noted that despite the success of field implementation of polymer gels in reducing CO2 fluxes, experimental work in support of laboratory-scale experiments was scattered, with varying results and parameters. The geological conditions and reservoir environments of different oilfields vary considerably, necessitating the development of a gel system suitable for the anti-CO<sub>2</sub> gas channeling. Nguele et al. (2021) developed a CO<sub>2</sub> thermo-responsive gel system using polyvinyl alcohol (PVOH) and silica (SiO<sub>2</sub>) nanoparticles, which is effective for anti-CO<sub>2</sub> gas channeling in heterogeneous formations, but not in matrix formations. Luo et al. (2023) conducted an investigation into the impact of an in-situ smart surfactant gel on anti-gas channeling during CO<sub>2</sub>-WAG. The results demonstrated that the gel effectively plugged the high permeability layer, thereby mitigating the gas channeling. Furthermore, the oil recovery rate was found to be 8% higher than that of the conventional WAG. Song et al. (2022) evaluated a pre-crosslinked particulate gel (CO2-BRPPG) for anti-CO<sub>2</sub> gas channeling purposes. The particles re-form into a viscous bulk gel after entering the reservoir, thereby achieving an effective plugging of the fracture to control gas channeling. The scholars referenced above have concentrated their efforts on CO2-responsive gel systems, encompassing both polymer-based and surfactant-based approaches. The transition of these novel materials from the laboratory to the oilfield requires further validation to ensure reliability. It is therefore necessary to develop more mature gel systems for the control of CO2 gas flushing. Gioia and Ciriello (2006) developed a non-toxic xanthan gum polymer gel system utilizing sodium aluminate as a cross-linking agent. However, the

gel is constrained in its applicability to high-temperature formations due to the utilization of xanthan gum biopolymers. Zhang et al. (2020) developed a polyacrylamide gel with a double crosslinking network formed by Cr(III) and phenolic resin. In comparison to gels containing only one crosslinking agent, polyacrylamide gels demonstrate enhanced thermal stability. The incorporation of a compound crosslinking system has been demonstrated to markedly enhance the temperature resistance of the gel. Bai et al. (2022) developed a polymer gel system that can withstand ultra-high temperatures (180 °C) for plugging ultra-deep wells for drilling. The gel has excellent temperature resistance properties and has good application prospects in the conventional reservoirs. Nevertheless, the system is susceptible to gel breakdown under acidic conditions, which is a disadvantage for its application in hightemperature acidic CO<sub>2</sub> flooding reservoirs. Consequently, the investigation of high temperature resistant (≥ 100 °C) gel systems suitable for CO2 acidity represents a pivotal aspect in the management of CO2 gas channeling in low permeability fractured reservoirs.

To overcome the high temperature and acidic formation conditions, a polymer gel system named AR-Gel was constructed based on a low hydrolysis, medium to high molecular weight polymer and a composite crosslinking system (phenolic resin and aluminium citrate). The gel was evaluated using the JL oilfield in China (90–100 °C) as the study object. The superiority of AR-Gel over conventional gels is demonstrated by the constitutive relationship between gel properties and microforms. The reservoir adaptability of AR-Gel was clarified by its properties and strength, and its acid resistance mechanism was revealed. Finally, the anti-CO<sub>2</sub> gas channeling effect of AR-Gel was evaluated by using a core physical simulation device, and the injection process of the gel was optimized. The research findings provide a high-temperature and acid-resistant anti-CO<sub>2</sub> gas channeling plugging agent material and construction process for low permeability oilfield.

#### 2. Materials and methods

#### 2.1. Materials

Industrial polymers (CN105, CN125, CX302, CX305, CX079, NE120, and SD120) and phenolic resin were provided by Qingdao Changxing Hi-tech Development Co., Ltd. Polyethyleneimine (PEI) is provided by Qingdao Huizhi Petroleum Technology Co., Ltd. Aluminum citrate, CaCl<sub>2</sub>, MgCl<sub>2</sub>·6H<sub>2</sub>O, NaHCO<sub>3</sub>, Na<sub>2</sub>SO<sub>4</sub>, and NaCl were all analytically pure and provided by China National Pharmaceutical Group Co., Ltd. The artificial cores were provided by China Marine Natural Core Co., Ltd, and the relevant parameters of the core are shown in Table S1 in Supplementary Material. N2 and CO<sub>2</sub> (> 99%) were purchased from Qingdao Devi Gas Co., Ltd. The crude oil is provided by JL oilfield in China, and its properties are shown in Table 1. The ionic composition of the simulated formation water from the JL oilfield is shown in Table 2. Deionized water was produced by double distillation in the (resistivity = 18.4 M $\Omega$ ·cm).

# 2.2. Methods

#### 2.2.1. Preparation of polymer gel

The polymer was slowly dissolved in formation water at pH=3 with a mechanical stirrer at 150 r/min for 2 h until complete dissolution. Then, the crosslinking agent was added to the homogeneous polymer solution, and  $N_2$  was passed into the polymer solution to create an anaerobic environment. Finally, the gel solution was transferred to an ampoule, sealed and placed in a thermostat.

**Table 1**Basic properties of crude oil in JL oilfield.

Density @ 100 °C, g/cm <sup>3</sup>	Viscosity @ 100 °C, mPa·s	Mass fraction, %	Mass fraction, %				
		Saturated hydrocarbon	Aromatic hydrocarbon	Resin	Asphaltene		
0.8303	1.16	62.58	23.98	13.16	0.28		

 Table 2

 Composition of simulated formation water in JL oilfield.

lon content, mg/L						Salinity, mg/L
Ca <sup>2+</sup>	$\mathrm{Mg}^{2+}$	Na <sup>+</sup>	HCO <sub>3</sub>	Cl <sup>-</sup>	SO <sub>4</sub> <sup>2-</sup>	
29.34	11.86	3641.66	2289.59	3852.71	703.16	10528.32

#### 2.2.2. Water loss rate and gel strength test

The variation of gel strength with time was observed using the inversion method (Yang et al., 2019), and the relationship between gel code and strength description is shown in Table S2 in Supplementary Material. The gel water loss rate was used to evaluate the long-term stability of the polymer gel. The gels were placed in a thermostat at 100  $^{\circ}$ C for an extended period of time, and the amount of water loss was recorded at different ageing times. The water loss rate (S) of the polymer gels was calculated using Eq. (1).

$$S = \frac{V - V_t}{V} \times 100\% \tag{1}$$

where S is the water loss rate, %; V is the volume of the gel at gelation, mL; and  $V_t$  is the volume of the gel after aging for time t, mL.

# 2.2.3. Pressure resistance value test

A vacuum tester was used to determine the pressure resistance value of the polymer gel (Lashari et al., 2018). One end of the U-tube was inserted 1 cm below the polymer gel, the vacuum pump was activated and the pressure at which the polymer gel was drawn from the U-tube into the conical flask was recorded as the pressure resistance value.

# 2.2.4. Microscopic morphology test

An environmental scanning electron microscope (ESEM) (PHI-LIPS, Holland) was employed to observe the microscopic morphology of polymer gels in the aqueous state. A high-speed electron beam emitted by an electron gun filament is focused by a mirror system and directed towards the area of the gel to be measured. The gel's microscopic morphology is then processed by the instrument's electronic system. The working distance is 11.084 mm and the magnification is 100 times. The accelerating voltage of the electron beam is 10 kV.

An atomic force microscope (AFM) (BRUKER, America) was used to test the apparent morphology of polymer gels. A small amount of gel was covered with a clean mica sheet and freeze-dried. The mica sheets were placed on a sample stage for characterization. For testing, the TESP probe and tap mode were selected and the experimental temperature was 25  $^{\circ}$ C.

#### 2.2.5. Rheology performance test

A micro-rheometer (FORMULACTION, France) was used to test the rheological properties during the gelation process. Tracer particles with a radius size of 50 nm were added to the gel solution and their trajectory directly reflects the gelling and rheological properties. The sample is loaded into a 20-mL cuvette and the sample height is controlled to be 2/3 of the cuvette. Backscattered light is

formed when the light from the laser source strikes the tracer particles in the sample. Due to the differing distances traversed by the tracer particles, a phase difference is observed, resulting in the diffraction of light of different phases, thereby forming light and dark scattering. A multi-pixel detector is employed to detect the fluctuations in the scattering in real time, with the velocity and mean square displacement (MSD) of the tracer particles subsequently calculated (Yang et al., 2018).

The macroscopic viscosity index (MVI) indicates the magnitude of the viscosity of the polymer gel system, while the elasticity index (EI) indicates the magnitude of the elasticity of the polymer gel system. The values of MVI and EI are calculated by Eqs. (2) and (3), respectively (Yang et al., 2016).

$$MVI = 1/k_{MSD}$$
 (2)

$$EI = 1/MSD (3)$$

where  $k_{\rm MSD}$  is the slope of the MSD curve during the third part of the de-correlation time; MSD is the MSD value in the central plateau region of the non-linear phase.

The flat plate system of the MCR301 rheometer (Anton Paar, Austria) with a PP43 rotor was employed to assess the viscoelasticity of polymer gels. The storage modulus (G') is the amount of energy stored by the elastic deformation of the gel in the oscillatory mode and characterizes the magnitude of elasticity. The loss modulus (G'') is the energy lost by the polymer gel due to viscous deformation and thus characterizes the magnitude of viscosity (Ramos et al., 2021). The test temperature was maintained at 25 °C, while the oscillation frequency ranged from 0.01 to 10 Hz.

The reversibility of the gel's creep behavior is also evaluated using the cone plate system. The phenomenon whereby a gel experiences a gradual deformation over time in the presence of a constant applied stress is known as creep. Upon the removal of the external force, the process of the gel returning to its initial state is referred to as recovery (Meharthaj et al., 2020). The temperature was set to 25 °C, the normal stress was 0.5 N, and the constant shear stress was 1 Pa. The dynamic testing process was divided into two steps. In the first step, the applied stress was maintained for 100 s, and in the second step, the withdrawal of the shear stress was recorded for 100 s. The change in strain over time was measured throughout the entire process.

# 2.2.6. Anti-CO<sub>2</sub> gas channeling and enhanced oil recovery test

To investigate the anti-CO<sub>2</sub> gas channeling ability of AR-Gel, cores with varying fracture widths were utilized. The experimental flow chart is depicted in Fig. 1. Initially, the core was saturated with formation water, and CO<sub>2</sub> was injected at a constant flow rate of 0.5 mL/min. Subsequently, a specific volume of gel solution

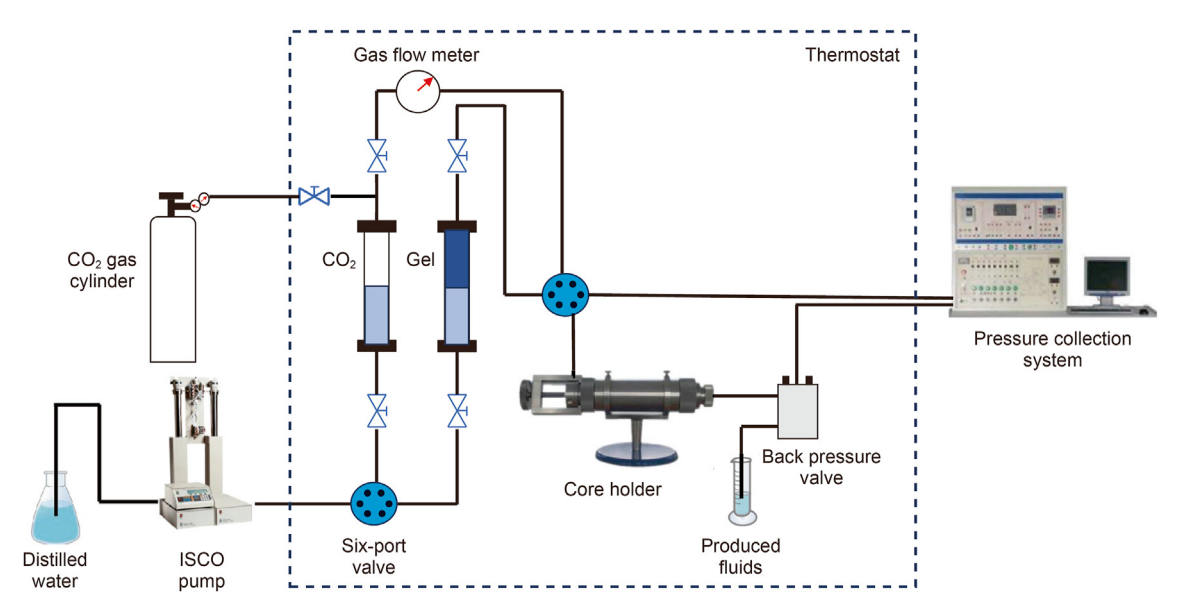


Fig. 1. Experimental device flow chart of anti-CO<sub>2</sub> gas channeling and enhanced oil recovery.

was injected following the stabilization of the gas drive pressure. The gel was then placed in a thermostat at 100 °C to facilitate the complete gelation process. Then,  $CO_2$  was injected at a constant rate, and the change in pressure with the injected volume was recorded throughout the entire process. The confining pressure of the core holder was maintained at 15 MPa, while the back pressure was set at 7.6 MPa. The effect of anti-gas channeling was quantified by the plugging rate  $(\eta)$ , which was calculated in accordance with Eq. (4).

$$\eta = \frac{k_1 - k_2}{k_1} \times 100\% \tag{4}$$

where  $\eta$  is the plugging rate, %;  $k_1$  is the permeability of the CO<sub>2</sub> flooding before gel injection,  $10^{-3} \, \mu \text{m}^2$ ;  $k_2$  is the permeability of the CO<sub>2</sub> flooding after gel injection,  $10^{-3} \, \mu \text{m}^2$ .

The  $CO_2$  enhanced recovery experiment, which follows the same procedure as the anti- $CO_2$  gas channeling experiment, differs from the latter in that the core used must be saturated with crude oil. The crude oil at the outlet is collected at regular intervals during the dynamic replacement process.

#### 3. Results and discussion

#### 3.1. Development and characterization of AR-Gel

Polymer is the most important component in the anti-CO<sub>2</sub> gas channeling polymer gel system. The probability of crosslinking with the crosslinking agent is higher for longer molecular chains, resulting in a higher crosslinking speed and density for the polymer gel. However, the use of polymers with an excessive molecular weight will impede the injection of the polymer gel system. The higher the degree of hydrolysis, the more carboxyl groups (—COOH) and the less amide groups (—CONH<sub>2</sub>) in the polymer chain. In general, an increase in the degree of hydrolysis of a polymer, which is reflected in an increase in the number of carboxyl groups, results in a faster gel formation time and a stronger gel. Conversely, a reduction in the degree of hydrolysis of a polymer, which is reflected in a reduction in the number of carboxyl groups, inhibits the hydration process of polymer molecules, resulting in a longer gel formation time (Liu et al., 2024). It should be noted that the acidic

environment created by the supercritical CO<sub>2</sub> flooding will cause the carboxyl group to hydrolyze and break, causing the polymer chain to shrink and lose a lot of water, leaving the gel susceptible to degradation and other adverse phenomena that will affect its plugging performance. As can be seen from the data for the gels in Fig. 2, polymer gels made from the medium to high molecular weight, low hydrolysis CX305 polymer have superior strength and ageing stability.

The properties of polymer gels produced with different crosslinking agents also vary. According to the preferred polymers with low degree of hydrolysis, the main organic crosslinking agents selected include polyethyleneimine (PEI) and phenolic resin (PR). Considering that there is still a part of carboxyl group in the polymer chain, a small amount of inorganic crosslinking agent can be added and aluminium citrate (AC), which has better acid resistance, is selected to form an organic/inorganic composite crosslinking agent to improve the temperature and acid resistance of the gel system (Fraga et al., 2020). As shown in Fig. 3, the composite crosslinking system formed by PR/AC has the best gel strength and aging stability. AC crosslinking agent with a small number of carboxyl groups on the polymer chain to form a preliminary network structure, and the gel strength formed by crosslinking is weak due to the low content of AC and carboxyl groups. On the other hand, the hydroxymethyl group (-CH<sub>2</sub>OH) on the PR and the amide group (-CONH<sub>2</sub>) in the polymer undergo a condensation reaction to make the polymer molecular chain form a solid spatial network structure, so the gel strength formed by this composite crosslinking system of organic and inorganic is the highest and the stability is the best.

Fig. 4 shows an environmental scanning electron microscope image of the AR-Gel at 30 days. It can be seen that the cluster-like three-dimensional network structure is clearly visible after 30 days of polymer gel aging, and the polymer chains are interwoven by crosslinking agents to form the skeleton of network pores, and these network pores are uniformly distributed and mutually supportive, which makes AR-Gel maintain high strength and stability in high-temperature acidic environments.

Fig. 5 shows the morphology of AR-Gel and phenolic resin gel observed under AFM. The peak heights of AR-Gel and phenolic resin gel are 893.8 and 538.7 nm, respectively, and the peak density of AR-Gel is larger than that of phenolic resin gel, indicating that the

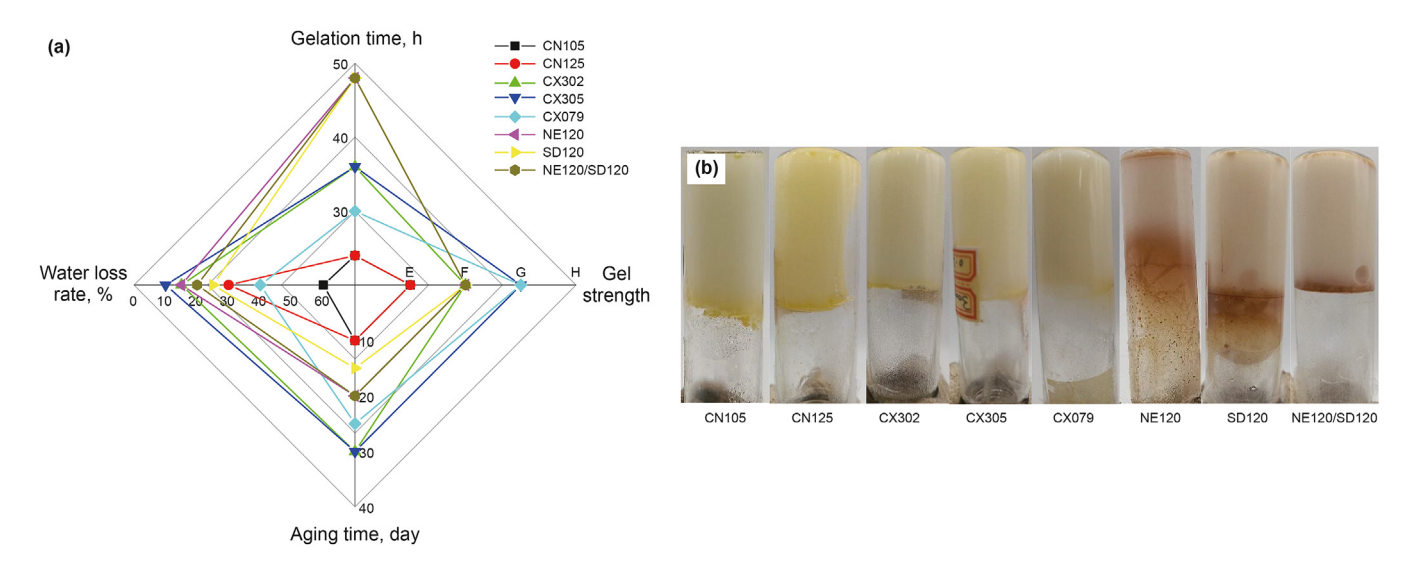


Fig. 2. Acid resistant gels prepared from different polymers: (a) polymer properties; (b) gel states.

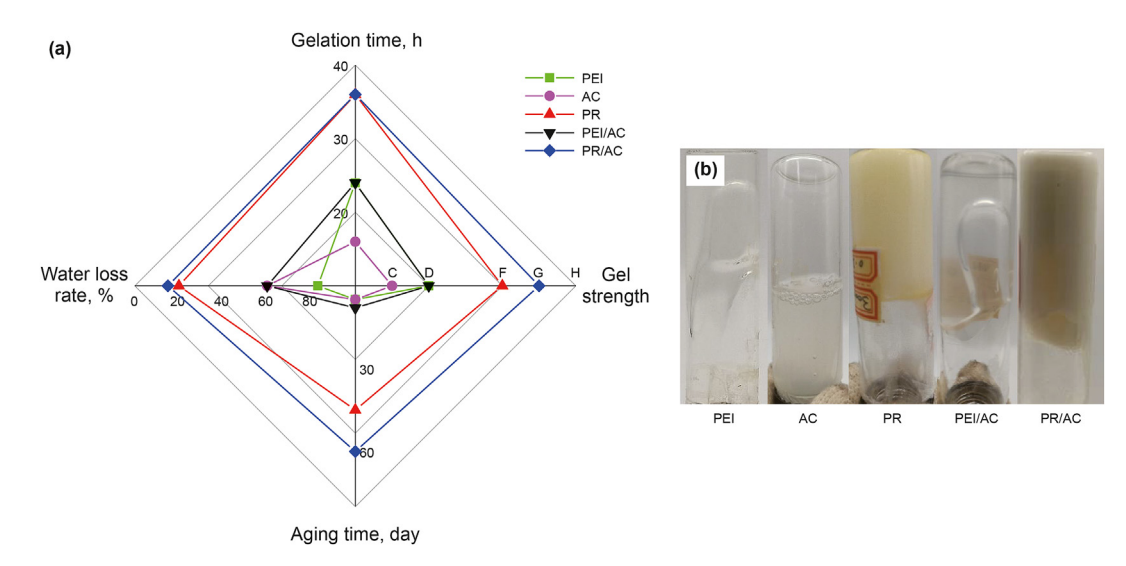


Fig. 3. Acid-resistant gels prepared with different crosslinking agents: (a) polymer properties; (b) gel states.

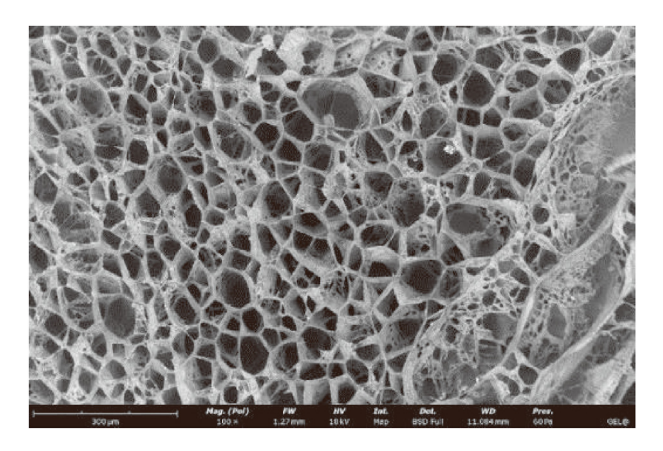


Fig. 4. Microscopic morphology of AR-Gel after 30 days of aging.

strength of the AR-Gel network is higher than that of phenolic resin gel, and the introduction of aluminium citrate increases the

network structure of the gel, so that the gel strength and stability was improved (Neto et al., 2024).

Based on the microrheological experiments during the polymer gelation process, the kinetic properties of the gels were studied and the results are shown in Fig. 6. The EI and MVI values of both gels increase and then stabilize over time due to the crosslinking reaction between the polymer and crosslinking agent, resulting in the appearance of a reticulated structure and gradual densification of the gel. This leads to a reduced range of motion of the tracer particles, which is reflected in the increased EI values on the images. At the same time, the resistance of the tracer particles also increases, which is reflected in an increase in the MVI value on the image. In terms of viscoelastic strength, the MVI and EI values of the AR-Gel are greater than that of the traditional phenolic resin gel, indicating that the addition of aluminium citrate improves the viscoelastic properties of the gel system, resulting in an increase in the strength and stability of the gel.

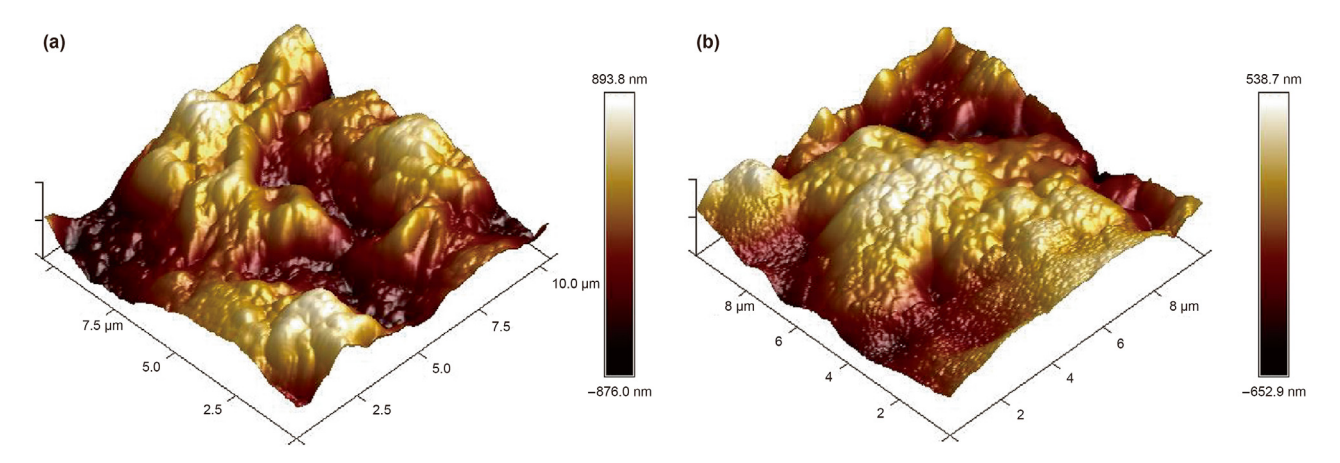


Fig. 5. AFM morphology of AR-Gel (a) and phenolic resin gel (b).

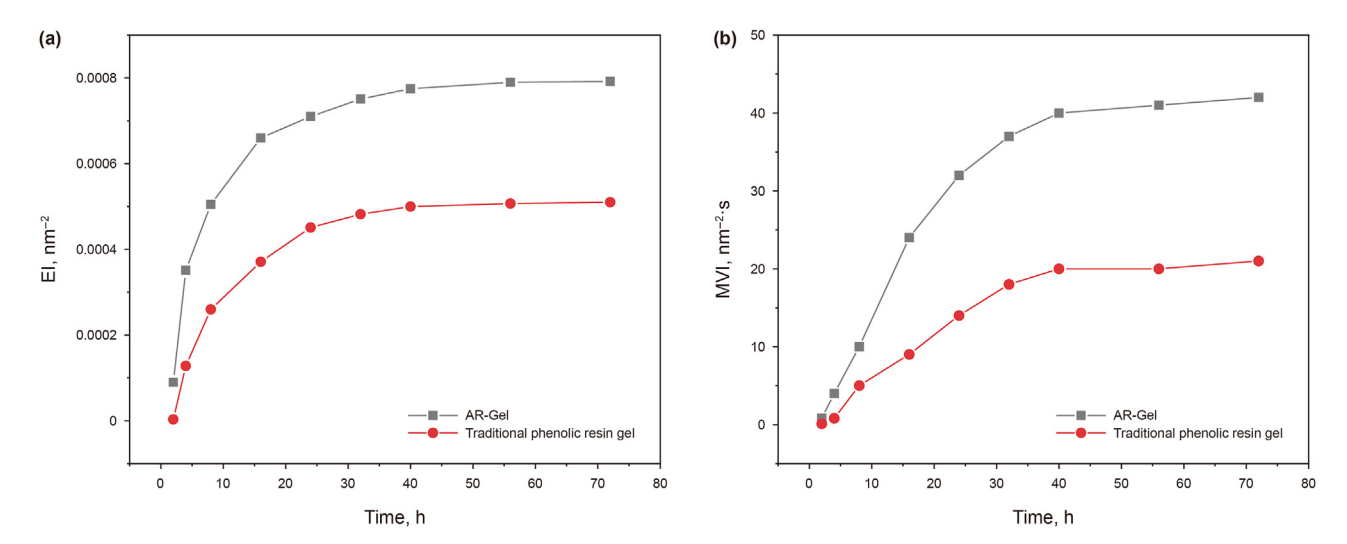


Fig. 6. Gelation kinetic properties of AR-Gel and phenolic resin gels: (a) EI; (b) MVI.

#### 3.2. Rheological properties of AR-Gel

The rheological properties of AR-Gel were investigated and compared with traditional phenolic resin gel (C-Gel) to reflect the viscoelasticity and compression recovery properties. The results of the viscoelasticity after gelation 30 days are shown in Fig. 7(a). The viscoelasticity of the AR-Gel was improved by the introduction of aluminium citrate, which enabled AR-Gel to maintain its high strength and stability. The results of the creep-recovery were shown in Fig. 7(b). Under the same force, the two gel systems deform rapidly at the creep stage, but the degree of deformation of the AR-Gel is smaller than that of the C-Gel at the same time, indicating that the AR-Gel is more capable of maintaining its gel properties under the action of external force. After the force is removed, the recovery ability of the AR-Gel is stronger and the stress has almost no effect on the structural properties of the gel system itself.

#### 3.3. Reservoir adaptability of AR-Gel

AR-Gel has higher strength properties than C-Gel, and further study of its strength changes under different influencing factors is beneficial to clarify its adaptability in harsh reservoirs.

#### 3.3.1. Temperature

Table 3 and Fig. 8 show the gel properties and strength of AR-Gel at different temperatures. At 110  $^{\circ}$ C, the water loss rate of AR-Gel reached 30% after 30 days, and the pressure resistance value and gel strength decreased significantly. At 115 °C, AR-Gel showed a large amount of water loss after 10 days, and could not even be formed into gel at 120 °C. There are two reasons for the weakening of AR-Gel strength above 110 °C. Firstly, the prolonged high temperature causes hydrolysis of the polymer molecules and hydrolysis of the amide groups to carboxyl groups, which hinders the crosslinking action of the phenolic resin. Secondly, the weak crosslinking effect formed by the carboxyl group and aluminium citrate is easily destroyed at high temperatures, and the carboxyl group undergoes a dehydration and condensation reaction with the amide group and hydroxymethyl group on the molecular chain, causing the molecular chain of the polymer gel to curl, the reticulation structure to shrink and the strength to decrease. The effect of temperature shows that at reservoir temperatures below 110 °C, AR-Gel has high strength and stability and can be effectively applied.

#### 3.3.2. Salinity

Table 4 and Fig. 9 illustrate the gel properties and viscoelasticity of AR-Gel under different salinity formation water. The data presented in the table indicates that as the salinity increased to

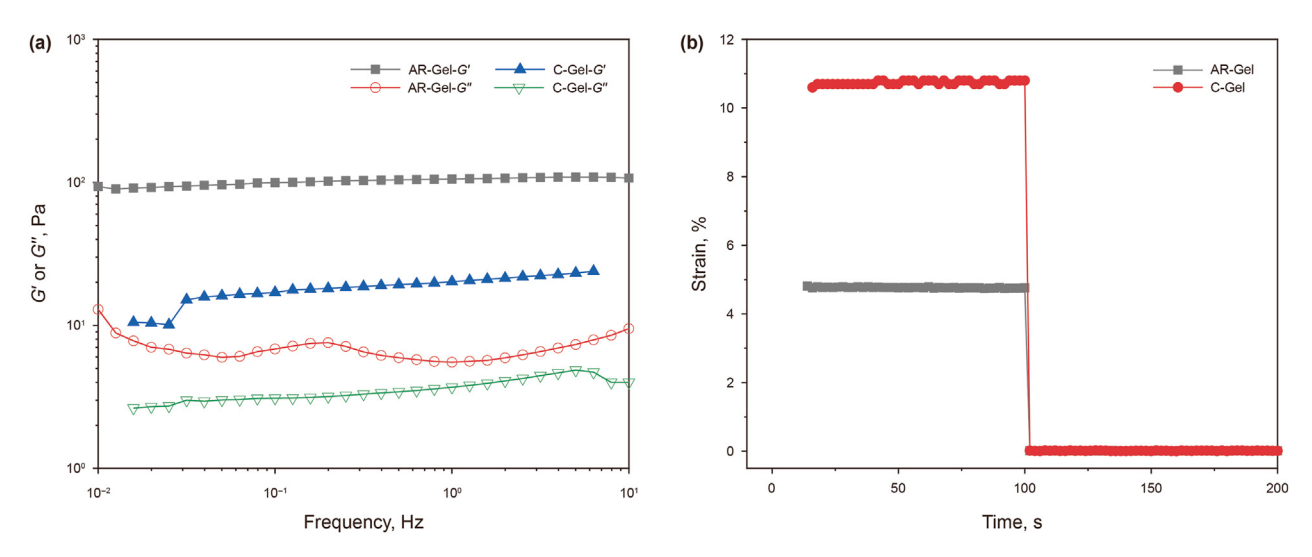


Fig. 7. Strength (a) and creep-recovery properties (b) of AR-Gel and C-Gel.

**Table 3** AR-Gel properties at different temperatures.

Temperature, °C	Gelation time, h	Gel strength	Aging time, day	Water loss rate, %	Pressure resistance value for 30 days, MPa
80	40	Н	30	0	0.070
90	40	Н	30	0	0.071
100	36	Н	30	0	0.068
105	34	Н	30	0	0.062
110	30	Н	30	30	0.038
115	28	I	10	35	_
120	No gelation	_	_	_	_

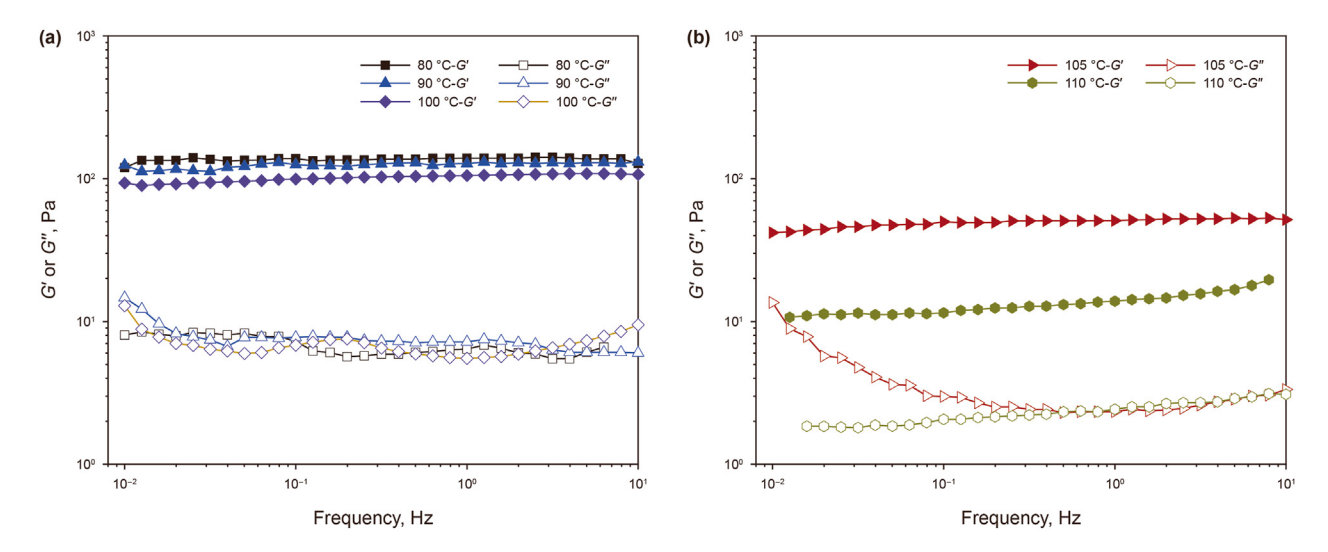


Fig. 8. Viscoelasticity of AR-Gel at different temperatures.

**Table 4**Gel properties of AR-Gel at different salinity.

Salinity, mg/L	Gelation time, h	Gel strength	Aging time, day	Water loss rate, %	Pressure resistance value for 30 days, MPa
12500	36	Н	30	0	0.062
15000	36	Н	30	0	0.058
17500	30	Н	30	10	0.051
20000	28	G	30	30	0.040

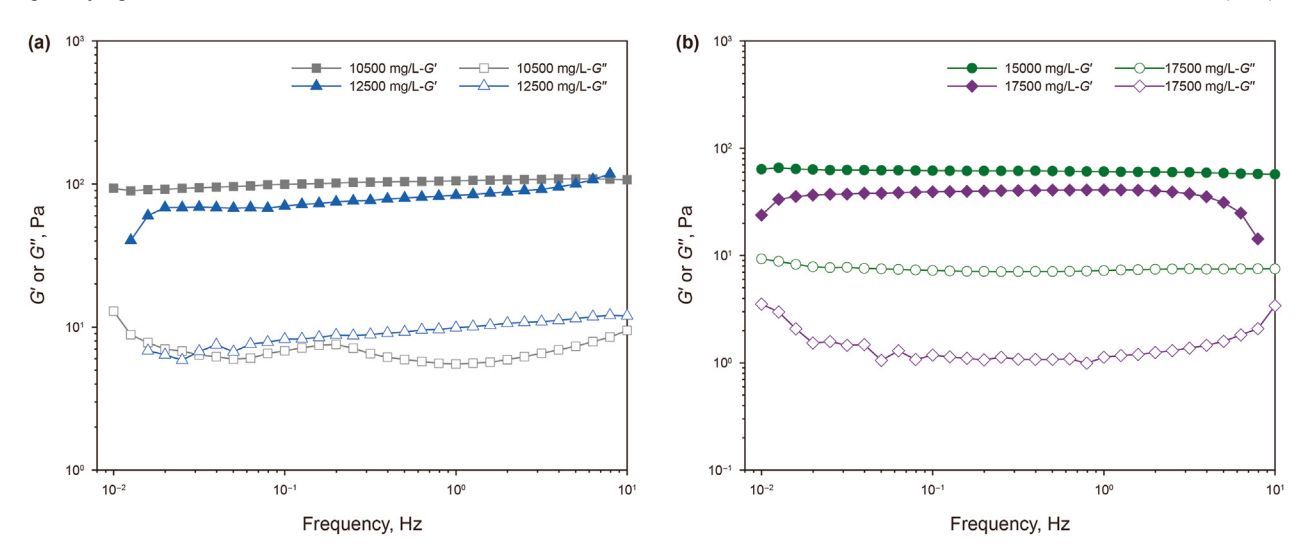


Fig. 9. Viscoelasticity of AR-Gel at different salinity.

15,000 mg/L, the gelation time exhibited a decreasing trend, accompanied by a water loss phenomenon and a concomitant decline in the pressure resistance value of the gel. The viscoelasticity of the gels exhibited a notable decline with increasing salinity, with a pronounced reduction occurring at a salinity of 17,500 mg/L. The acceleration of the gelation time with the salinity increase is attributed to the rise in the concentration of inorganic salt ions, which makes the compression of the diffuse bilayer of ionic groups in the polymer molecular chain more severe. Therefore, the chains of polymer molecules are less repulsive and curl around each other. The proximity of the crosslinking groups to each other makes it easier for crosslinking reactions to occur between the molecular chains, resulting in faster cross-linking. At this stage, the hydrodynamic volume occupied by the polymer molecules is minimal, and excessive crosslinking between molecules results in a highly dense mesh structure, which causes the original water-wrapped spatial mesh structure of the gel to extrude, leading to a serious loss of water within the gel. This subsequently results in a decline in the stability and viscoelasticity of the gel. Therefore, AR-Gel is suitable for reservoir environments below 20,000 mg/L salinity.

#### 3.3.3. Shear action

Table 5 and Fig. 10 illustrate the properties and viscoelasticity of AR-Gel following shearing for 3 min at varying shear rates. Following the shear forces at varying rates, the gelation time of the gels exhibited a corresponding increase with the rise in shear rate. Furthermore, the viscoelastic curve indicates that the viscoelasticity of the gel diminishes with an augmenting shear rate. This phenomenon can be attributed to the entanglement of polymer molecular chains in the gel solution at low shear rates. External forces then act upon these chains, resulting in movement and relaxation, which leads to an increase in the intermolecular gravitational force. As the shear rate is increased, the polymer molecular chain is damaged by shear, resulting in the phenomenon of shear

dilution. This leads to a deterioration in the performance of the gel and a reduction in its viscoelasticity after the gelation. AR-Gel exhibits superior shear resistance and is capable of maintaining its plugging performance after shear.

#### 3.3.4. Oil content

After AR-Gel is injected into the formation, the gel solution will preferentially enter into gas channeling channels such as fractures with little crude oil content, so the effect of crude oil on AR-Gel gel properties and viscoelasticity was explored by adding a small amount of crude oil. The effects of varying crude oil contents on the gel properties and viscoelasticity of AR-Gel are presented in Table 6 and Fig. 11. The gel properties and viscoelasticity of AR-Gel exhibited minimal variation when the crude oil content was low. The polymer and crosslinking agent are dispersed in the gel solution. The gel solution and the oil phase are separated from each other due to the low density of the crude oil and the different polarity of the aqueous phase. The presence of crude oil does not affect the crosslinking reaction of polymers and crosslinking agents in the aqueous phase during the gelation process. Consequently, the crude oil remains in the form of two phases even after gelation. As the proportion of crude oil in the AR-Gel solution increases, the gel properties remain satisfactory, although the gel strength is observed to decrease.

#### 3.4. Performance of AR-Gel under supercritical CO<sub>2</sub>

The prepared gel solution was placed in an acid-resistant ageing stability container. A  $CO_2$  pressure of 7 MPa was then passed into the container and placed in a 100 °C thermostat to simulate a supercritical  $CO_2$  environment. The rheological properties of the gel were then tested at 10, 30, and 60 days of gel formation, respectively (Sun et al., 2018). The viscoelastic of AR-Gel at different times are shown in Fig. 12. The viscoelasticity of the gel was high at day

**Table 5**Gel properties of AR-Gel at different shear rates.

Shear rate, r/min	Gelation time, h	Gel strength	Aging time, day	Water loss rate, %	Pressure resistance value for 30 days, MPa
4000	36	Н	30	0	0.062
6000	40	Н	30	0	0.063
8000	48	G	30	5	0.059
10000	48	G	30	10	0.052

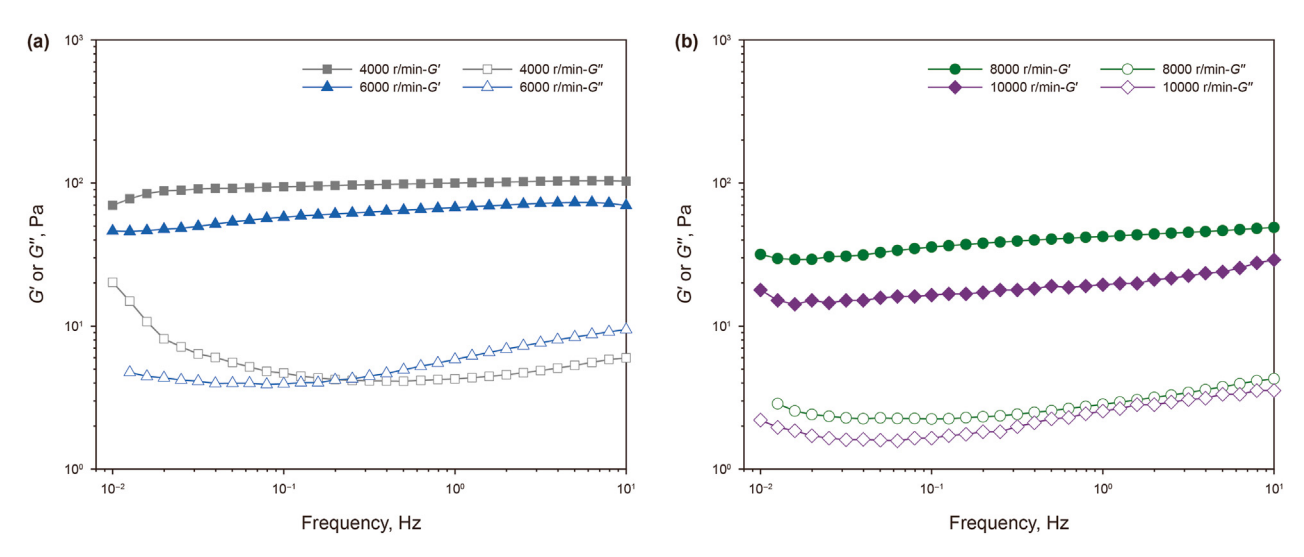


Fig. 10. Viscoelasticity of AR-Gel after different shear rates.

**Table 6**AR-Gel properties at different crude oil contents.

Crude oil content, %	Gelation time, h	Gel strength	Aging time, day	Water loss rate, %	Pressure resistance value for 30 days, MPa
0	36	Н	30	0	0.068
10	36	Н	30	0	0.063
20	40	G	30	5	0.049

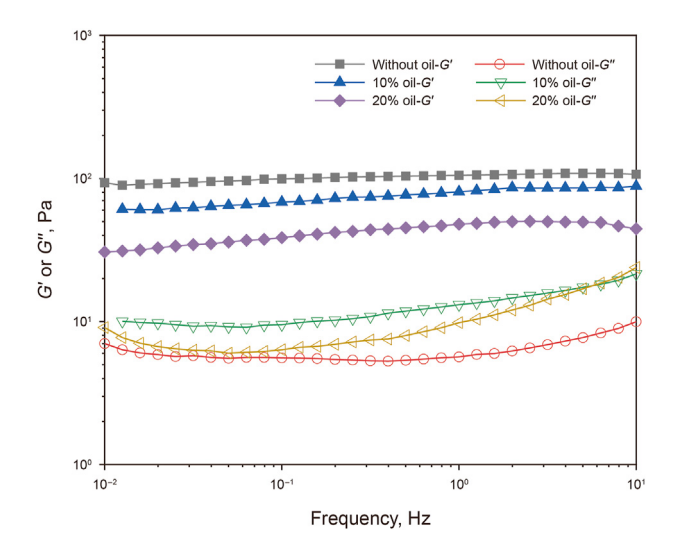
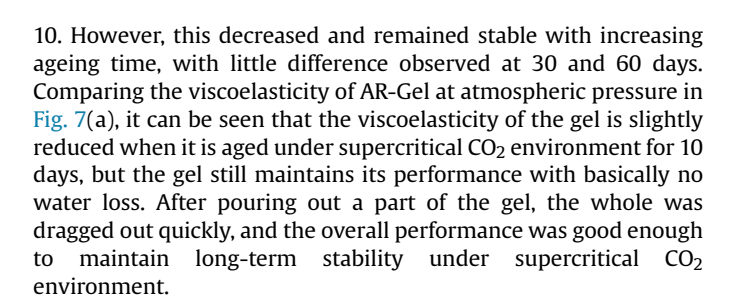


Fig. 11. Viscoelasticity of AR-Gel at different oil contents.



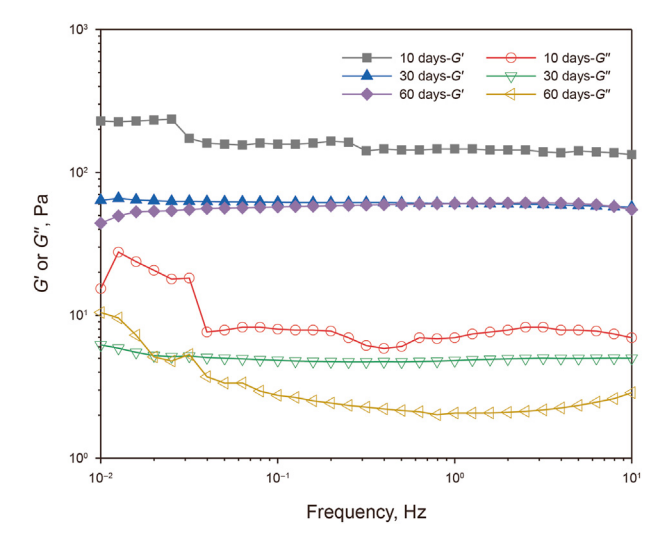


Fig. 12. Viscoelasticity of AR-Gel at different times in supercritical CO<sub>2</sub> environment.

# 3.5. Double crosslinking and acid resistance mechanism

Based on the observation results of rheology and bottle test method, the gelation and acid resistance mechanism of AR-Gel is summarized as shown in Fig. 13. Firstly, aluminium citrate is an inorganic crosslinking agent suitable for acidic conditions. It undergoes ionization in aqueous solution to produce citrate ions and trivalent aluminium ions (Al(III)). In solution, citrate ions form a diffuse double layer, with hydrogen ions acting as counter ions around the citrate. This prompts the ionization of the carboxyl

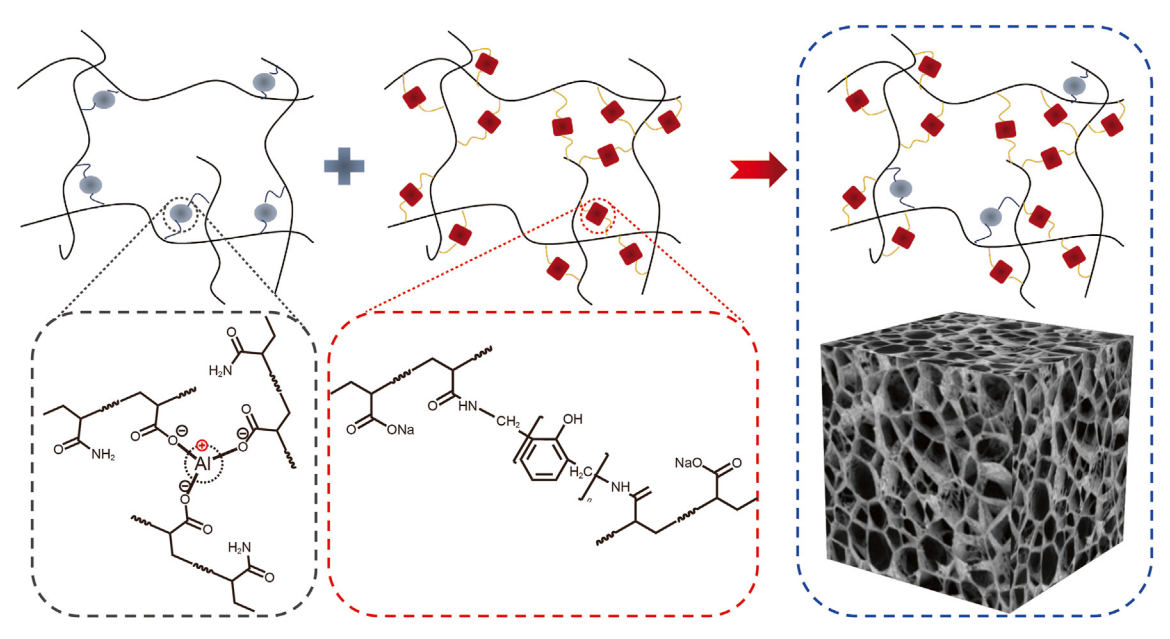


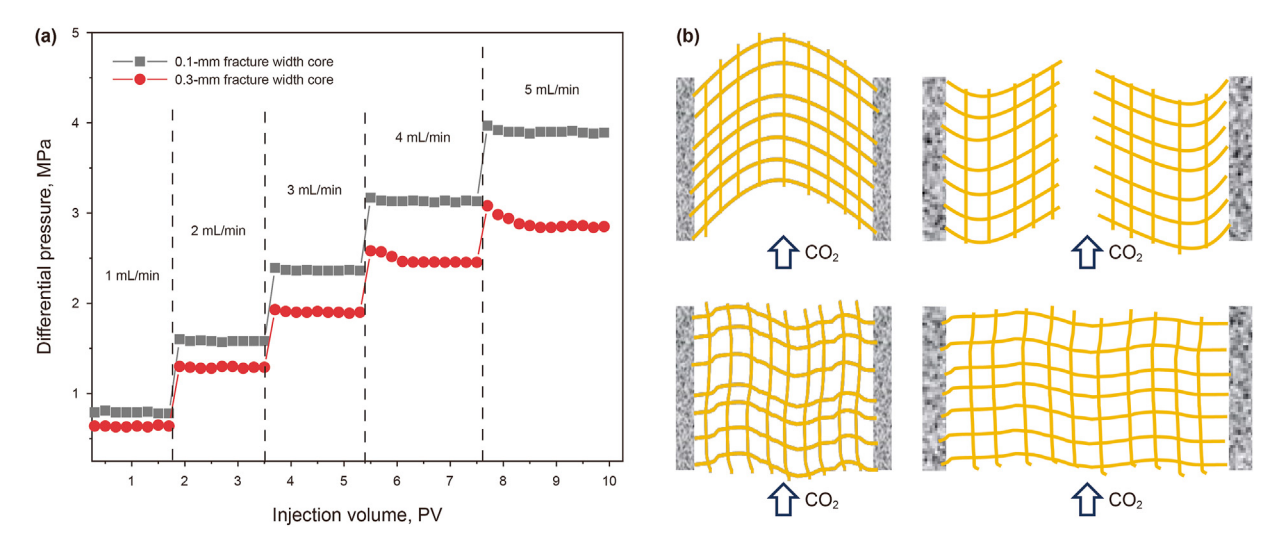
Fig. 13. Gel formation and acid resistance mechanism of AR-Gel.

**Table 7**Plugging effect of AR-Gel in fractured cores with different seam widths.

Core number	Fracture width, mm	CO <sub>2</sub> injecting before the gel		CO <sub>2</sub> injecting after the gel	Plugging rate, %	
		Differential pressure, MPa	Permeability, 10 <sup>-3</sup> μm <sup>2</sup>	Differential pressure, MPa	Permeability, $10^{-3} \ \mu m^2$	
D-1	0.05	0.011	154.4	0.393	4.32	97.2
D-2	0.10	0.010	169.9	0.396	4.29	97.5
D-3	0.15	0.009	188.7	0.369	4.60	97.6
D-4	0.20	0.007	242.6	0.353	4.81	98.0
D-5	0.30	0.005	339.7	0.323	5.26	98.5

groups on the polymer molecular chains. The Al(III) is formed through hydrolysis and a hydroxyl bridge reaction, resulting in the formation of a strong, positively charged polynuclear hydroxyl bridge complex ion. Al(III) is then able to crosslink with the negatively charged carboxyl group on the polymer molecular chain, thereby forming the first layer of gel (Fraga et al., 2020). Then, the polymer CX305 has a lower degree of hydrolysis and fewer carboxyl

groups in its molecular chain. Furthermore, the aluminium citrate crosslinking agent reacts more rapidly with the polymer, thereby reducing the distance between the phenolic resin and the polymer molecular chain. The collision frequency of the phenolic resin with the amide group on the polymer chain is increased, thereby enhancing the likelihood of a crosslinking reaction. In conclusion, the gel mesh structure that was formed following the process of



 $\textbf{Fig. 14.} \ \ \text{Differential pressure curves (a) and gel states (b) in the fracture core with different widths.}$ 

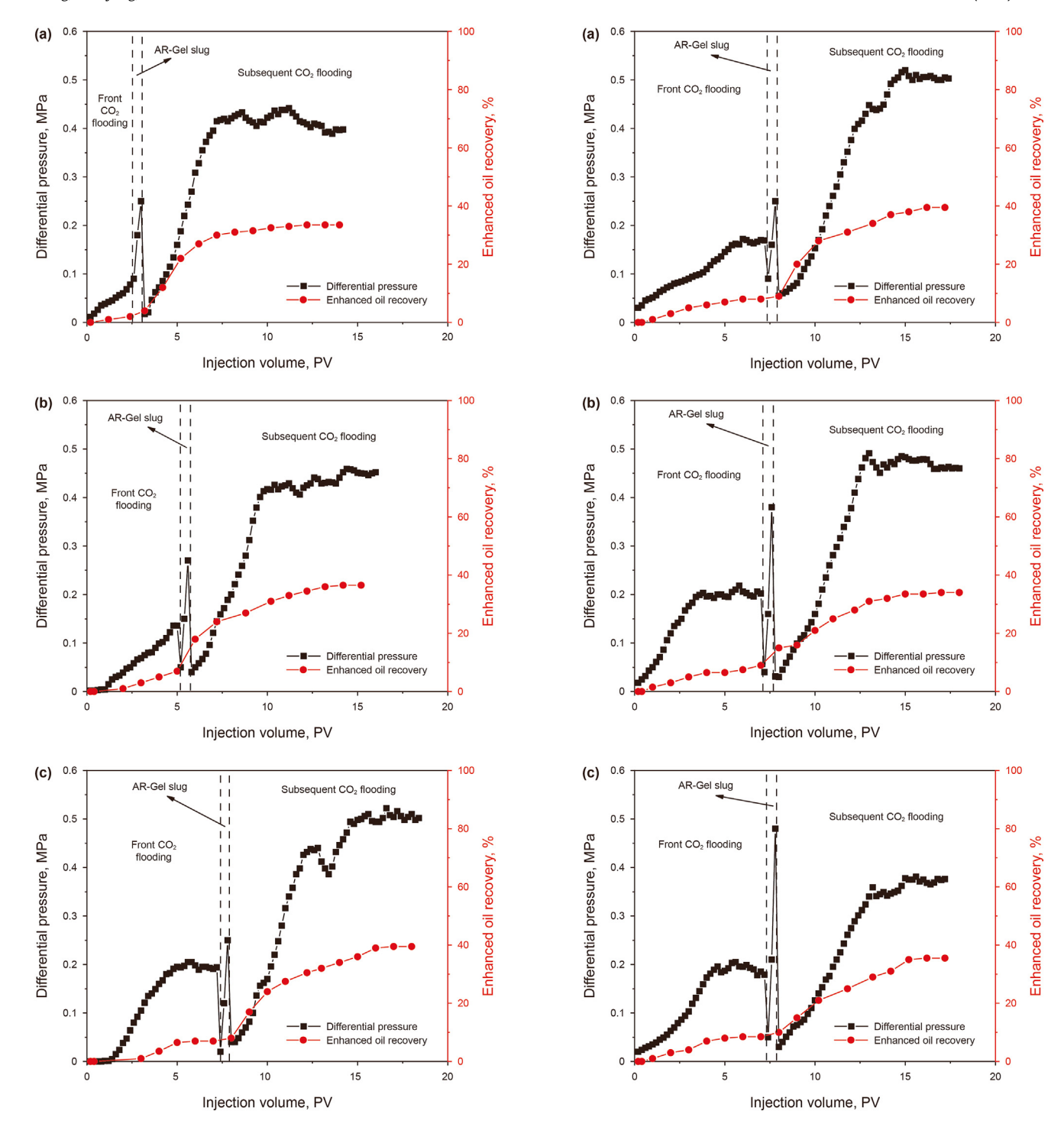


**Fig. 15.** Production dynamic of AR-Gel plug with different injection time: (a) just seeing gas; (b) gas—oil ratio  $20~\text{m}^3/\text{m}^3$ ; (c) gas—oil ratio  $100~\text{m}^3/\text{m}^3$ .

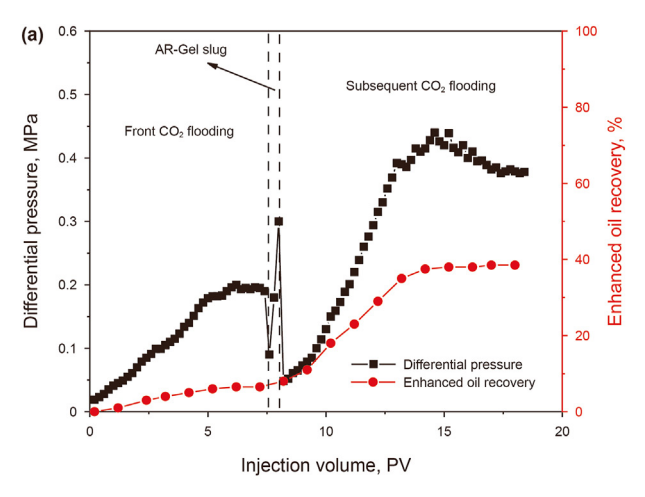
Fig. 16. Production dynamics of AR-Gel plug at different injection rates: (a) 0.5 mL/min; (b) 1.0 mL/min; (c) 2.0 mL/min.

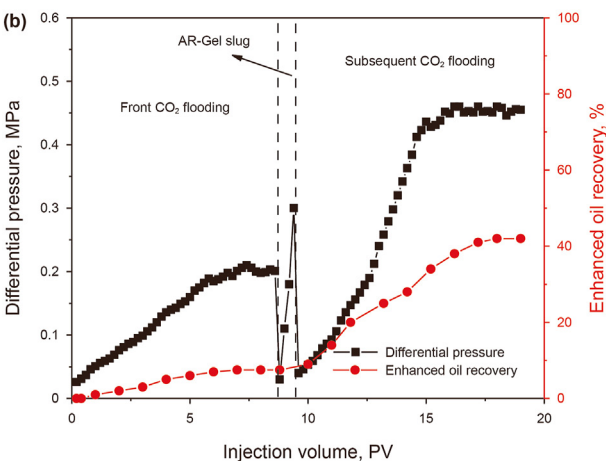
**Table 8**Crude oil recovery with different injection time.

Core number	Injection time (gas—oil ratio)	Extraction degree of oi	Extraction degree of oil, %		
		Front CO <sub>2</sub> flooding	AR-Gel slug	Subsequent CO <sub>2</sub> flooding	
D-8	0	2.0	5.0	33.5	31.5
D-9	20	5.0	7.0	36.5	31.5
D-10	100	7.0	8.0	40.0	33.0

**Table 9**Crude oil recovery with different injection rates.

Core number	Injection rate, mL/min	Extraction degree of oil	Extraction degree of oil, %				
		Front CO <sub>2</sub> flooding	AR-Gel slug	Subsequent CO <sub>2</sub> flooding			
D-11	0.5	8.0	9.0	39.5	31.5		
D-12	1.0	7.0	8.5	37.0	30		
D-13	2.0	8.5	10	35.5	27		





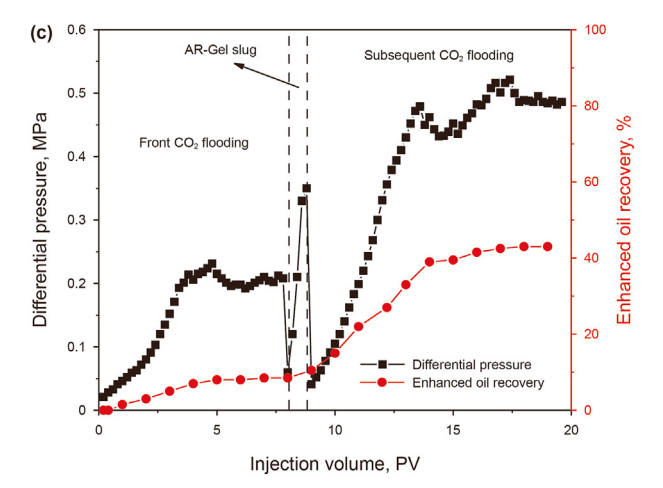


**Fig. 17.** Production dynamic of AR-Gel plug at different injection volumes: (a) 0.6 PV; (b) 0.8 PV; (c) 1.0 PV.

double crosslinking exhibited greater density, enhanced strength and stability, and was thus able to maintain long-term stability in a supercritical CO<sub>2</sub> acidic environment.

# 3.6. Anti-CO<sub>2</sub> gas channeling effect in fracture core

As demonstrated in Table 7, the anti- $\mathrm{CO}_2$  gas channeling effect of AR-Gel in fractured cores with varying fracture widths was evaluated. When the  $\mathrm{CO}_2$  injection rate was maintained at a constant level, AR-Gel demonstrated the capacity to effectively plug fractured cores with fracture widths of 0.05–0.30 mm, exhibiting a plugging rate of approximately 98% and a pronounced anti- $\mathrm{CO}_2$  gas channeling effect.

To further investigate the plugging stability of AR-Gel in fractured cores, variable flow rate injection experiments were carried out to investigate the plugging performance of the gel under the dual effects of different fracture widths and injection rates, and the results are shown in Fig. 14(a). In the 0.1-mm width fracture core, the pressure increased with the increase in injection speed, and the pressure was relatively stable, indicating that the high-speed gas flow did not result in excessive deformation and transport of the gel, and that the gel plugging performance was excellent. In the 0.3mm width fracture core, following an injection rate exceeding 3 mL/min, the pressure initially declines before stabilizing. This indicates that the gel is subjected to deformation and transport under the influence of high-speed airflow, resulting in a certain degree of gas channeling. Consequently, the plugging performance of the gel is compromised. Therefore, when utilizing AR-Gel for the construction of anti-CO<sub>2</sub> gas channeling, it is imperative that the gas injection rate be regulated to a maximum of 3 mL/min. Alternatively, in micro-fractured reservoirs with a fracture width of less than 0.1 mm, the AR-Gel may be employed. Fig. 14(b) illustrates the schematic diagram of the gel state when CO<sub>2</sub> passes through large and small fractures. It can be observed that the gel is relatively resistant to deformation in small fractures and exhibits high impact strength. In the case of a large fracture, the middle section of the gel is particularly susceptible to erosion by the high-speed gas, which can lead to a deterioration in the gel plugging efficacy.

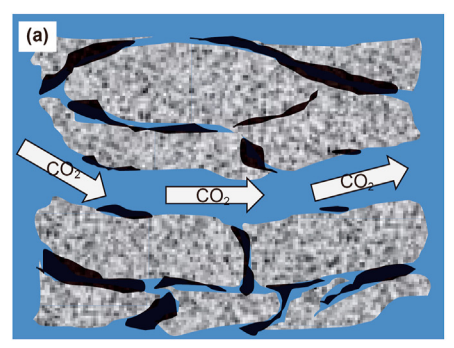
# 3.7. Process optimization of anti-CO<sub>2</sub> gas channeling for AR-Gel

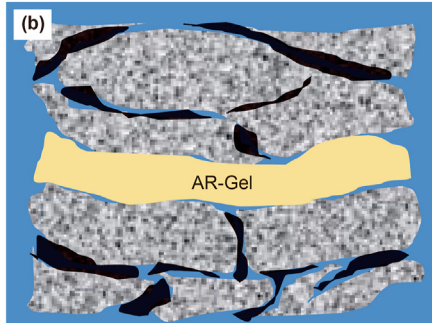
# 3.7.1. Injection time

By changing the segment plug size of the front  $CO_2$  flooding, the effect of different injection time on the recovery enhancement of  $CO_2$  flooding after AR-Gel plugging was investigated. By monitoring the production gas—oil ratio to control the injection timing, AR-Gel was injected when the gas was just seen at the extraction end and the gas—oil ratios were 20 and 100 m³/m³, respectively, and the production dynamic curves are shown in Fig. 15, and the recovery rates of each stage are shown in Table 8. With the increase in gas content at the outlet end, the injection volume of the front  $CO_2$  flooding increases, and its maximum differential pressure also increases. When the gas was just seen at the outlet end with the gas—oil ratio of  $20 \text{ m}^3/\text{m}^3$ , the front  $CO_2$  flooding was not yet fully stabilized, at which time the recovery rates were 33.5% and 36.5%,

**Table 10**Crude oil recovery with different injection volumes.

Core number	Injection volume, PV	Extraction degree of oil	Extraction degree of oil, %			
		Front CO <sub>2</sub> flooding	AR-Gel slug	Subsequent CO <sub>2</sub> flooding		
D-14	0.6	6.5	8.0	38.5	32.0	
D-15	0.8	7.5	9.0	42.0	34.5	
D-16	1.0	8.5	10.5	43.0	34.5	





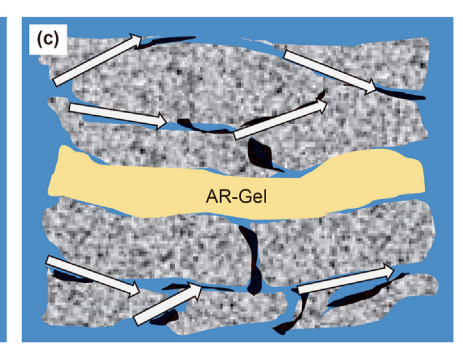


Fig. 18. The mechanism of AR-Gel for anti-CO<sub>2</sub> gas channeling and CO<sub>2</sub> enhanced oil recovery.

respectively. When the gas—oil ratio reaches  $100 \text{ m}^3/\text{m}^3$ , the front  $CO_2$  flooding has driven out the crude oil in the dominant channel, the pressure is stable. At this time, the injected AR-Gel can completely plug the fracture, and the subsequent  $CO_2$  flooding can drive more crude oil from the matrix. Accordingly, the decision has been taken to inject AR-Gel when the gas—oil ratio reaches  $100 \text{ m}^3/\text{m}^3$ .

#### 3.7.2. Injection speed

The injection speed of the gel solution not only affects the transport pattern in the formation pore, but also changes the shear effect on the gel and affects its gelation time. A faster injection rate will allow the gel solution to reach the formation faster for crosslinking and plugging, thus reducing the time and cost, but it will also reduce the gel strength. The AR-Gel injection rates were 0.5, 1, and 2 mL/min, and the production dynamics are shown in Fig. 16, and the recovery rates at each stage are shown in Table 9. With the increase in injection rate, the pressure of the gel plug rises faster, the gel solution is subjected to strong shear, and the gel strength in the core becomes lower. This results in a decrease in the plugging ability of the gel, which in turn reduces the improvement level in oil recovery rate. The gelation time of the AR-Gel is at 40 h, and the gel solution can be transported to a more distant target formation for plugging at an injection rate of 0.5 mL/min, so it is preferred that the injection rate of the AR-Gel is 0.5 mL/min.

### 3.7.3. Injection volume

An increase in injection volume will result in an expansion of the plugging area of the gel, with a corresponding increase in the plugging effect. Nevertheless, an injection volume that is excessively high may result in the plugging of oil-bearing pores or the direct flow of the gel solution out of the outlet end, thereby increasing the associated costs. The injection volume of AR-Gel was selected as 0.6, 0.8, and 1.0 PV, and the production dynamics are shown in Fig. 17, and the recovery rates of each stage are shown in Table 10. The oil recovery from the subsequent CO<sub>2</sub> flooding can reflect the effect of the injection volume of AR-Gel, when the injection volume was increased to 0.8 PV, the recovery increased by 2.5%, while the improved recovery when the injection volume was continued to be added to 1.0 PV did not continue to increase, which

indicated that the extra gel could not increase the anti- $CO_2$  gas channeling performance, so the injection volume of AR-Gel was selected to be 0.8 PV.

In summary, the optimal injection parameters for AR-Gel are injection when the gas—oil ratio at the outlet end reaches  $100~\text{m}^3/\text{m}^3$ , the injection rate is 0.5 mL/min, and the injection volume is 0.8 PV, at which time the enhanced recovery of  $CO_2$  flooding is 34.5%.

#### 3.8. Anti-CO<sub>2</sub> gas channeling mechanism

The anti-CO2 gas channeling mechanism of AR-Gel was proposed through CO2 flooding plugging and enhanced oil recovery experiments. Fig. 18(a) shows the front CO<sub>2</sub> flooding enhanced oil recovery process. The presence of fractures makes CO<sub>2</sub> undergo gas channeling, which only flows along the high permeability channels such as fractures and large pores, and is unable to reach the residual oil in other pore channels which are low permeability. In Fig. 18(b), the gel solution preferentially is transferred into the oil-free dominant channel (fracture) formed after CO2 flooding, and undergoes subsurface crosslinking to form a high-strength AR-Gel at reservoir temperature. The spatial network structure of the gel is sufficiently tight to firmly adsorb in the fracture, which can adapt to high temperature and acidic supercritical CO<sub>2</sub> environment, plugging the fracture completely, and improving the heterogeneous of the reservoir. Fig. 18(c) shows the process of subsequent CO<sub>2</sub> flooding after AR-Gel plugging, as the dominant channel is blocked, the gel can remain stable under CO<sub>2</sub> scouring. CO<sub>2</sub> is diverted to the oil-bearing pores that are not blocked by the gel, forming a new gas-drive channel, and the gas flow distribution ratio in the matrix core rises, which increases the swept volume of the CO<sub>2</sub>, and then plays a role in the effect of anti-CO<sub>2</sub> gas channeling and enhanced oil recovery.

# 4. Conclusions

Aim to the  $CO_2$  gas channeling problem in the JL oilfield in China, a new temperature resistance and acid resistant gel plugging system named AR-Gel was developed. This new material is intended to provide a solution for the anti- $CO_2$  flooding channeling and

#### conformance control in oilfields.

- (1) A gel named AR-Gel formed from a medium to high molecular weight, low hydrolysis polymer CX305 with a composite crosslinking system (phenolic resin/aluminium citrate) was developed. The gel strength reached H with a pressure resistance value of 0.066 MPa at 100 days.
- (2) AR-Gel has excellent reservoir adaptability to meet supercritical  $\rm CO_2$  reservoirs at 110 °C and 20,000 mg/L salinity, with strong shear resistance and long-term stability of more than 60 days.
- (3) The first layer network gel is composed of Al(III) and carboxyl group. Phenolic resin forms a second network gel with higher strength by crosslinking with amide groups. The tightly packed dual network gel enables AR-Gel to maintain superior performance under acidic conditions.
- (4) The best construction parameters of AR-Gel were selected, and the plugging rate of the gel under this process reached 97%. Subsequent CO<sub>2</sub> flooding increased the oil recovery rate by 34.5%, and the AR-Gel effectively controlled the CO<sub>2</sub> gas channeling and enhanced oil recovery.

#### **CRediT authorship contribution statement**

Hong-Bin Yang: Writing — review & editing, Writing — original draft, Project administration, Funding acquisition, Formal analysis, Data curation. Hai-Zhuang Jiang: Writing — review & editing, Writing — original draft, Methodology, Formal analysis, Data curation. Zhe Xu: Formal analysis, Data curation. Xing Zhang: Project administration, Investigation. Tao Wang: Writing — review & editing. Hai-Ning Liu: Methodology, Investigation. Xiao Ma: Methodology. Jian-Jun Zhu: Supervision. Xiang-Feng Zhang: Writing — original draft. Wan-Li Kang: Writing — review & editing, Resources, Project administration.

#### **Declaration of competing interest**

No conflict of interest exits in the submission of this manuscript, and manuscript is approved by all authors for publication. I would like to declare on behalf of my co-authors that the work described was original research that has not been published previously, and not under consideration for publication elsewhere, in whole or in part. All the authors listed have approved the manuscript that is enclosed.

#### **Acknowledgements**

The project was supported by the Fund of State Key Laboratory of Deep Oil and Gas, China University of Petroleum (East China) (No. SKLDOG2024-ZYRC-06), Key Program of National Natural Science Foundation of China (52130401), National Natural Science Foundation of China (52104055, 52374058), and Shandong Provincial Natural Science Foundation, China (ZR2021ME171, ZR2024YQ043).

#### Appendix A. Supplementary data

Supplementary data to this article can be found online at https://doi.org/10.1016/j.petsci.2024.11.016.

#### References

Bai, Y., Liu, C., Sun, J., et al., 2022. Use of a polymer gel for killing a high-temperature and high-pressure gas well. SPE J. 27 (6), 3297—3313. https://doi.org/10.2118/210586-PA.

Brattekås, B., Seright, R., 2023. A review of polymer gel utilization in carbon dioxide flow control at the core and Field Scale. SPE J. 28 (6), 3291–3307. https://doi.org/10.2118/217427-PA.

- Cui, C., Wei, S., Wang, Z., et al., 2022. Response time of waterflooding in low-permeability reservoirs. Unconventional Resources 2, 85–90. https://doi.org/10.1016/j.uncres.2022.08.003.
- Davoodi, S., Al-Shargabi, M., Wood, D.A., et al., 2024. Carbon dioxide sequestration through enhanced oil recovery: a review of storage mechanisms and technological applications. Fuel 366, 131313, https://doi.org/10.1016/i.fuel.2024.131313.
- Ding, Y., Zhao, Y., Wen, X., et al., 2023. Development and applications of CO<sub>2</sub>-responsive Gels in CO<sub>2</sub> flooding and geological storage. Gels 9 (12), 936. https://doi.org/10.3390/gels9120936.
- Dogah, B., Atashbari, V., Ahmadi, Mohabbat, et al., 2021. Enhanced oil recovery using CO<sub>2</sub> in alaska. Geosciences 11 (2), 98. https://doi.org/10.3390/geosciences11020098.
- Fraga, A.K., Oliveira, P.F., das Dores, F.G.L., et al., 2020. Synthesis and characterization of aluminum citrate compounds and evaluation of their influence on the formation of hydrogels based on polyacrylamide. Iran. Polym. J. (Engl. Ed.) 29 (8), 649–657. https://doi.org/10.1007/s13726-020-00825-5.
- Gandomkar, A., Torabi, F., Riazi, M., 2021. CO<sub>2</sub> mobility control by small molecule thickeners during secondary and tertiary enhanced oil recovery. Can. J. Chem. Eng. 99 (6), 1352–1362. https://doi.org/10.1002/cice.23936.
- Gioia, F., Ciriello, P.P., 2006. The containment of oil spills in porous media using xanthan/aluminum solutions, gelled by gaseous CO<sub>2</sub> or by AlCl<sub>3</sub> solutions. J. Hazard Mater. 138 (3), 500–506. https://doi.org/10.1016/j.jhazmat.2006.05.095.
- Hao, H., Hou, J., Zhao, F., et al., 2016. Gas channeling control during CO<sub>2</sub> immiscible flooding in 3D radial flow model with complex fractures and heterogeneity. J. Petrol. Sci. Eng. 146, 890–901. https://doi.org/10.1016/j.petrol.2016.07.034.
- Jansen-van Vuuren, R.D., Naficy, S., Ramezani, M., et al., 2023. CO<sub>2</sub>-responsive gels. Chem. Soc. Rev. 52 (10), 3470–3542. https://doi.org/10.1039/D2CS00053A.
- Jiang, H., Kang, W., Li, X., et al., 2021. Stabilization and performance of a novel viscoelastic N<sub>2</sub> foam for enhanced oil recovery. J. Mol. Liq. 337, 116609. https:// doi.org/10.1016/j.molliq.2021.116609.
- Jiang, H., Yang, H., Pan, R., et al., 2024. Performance and enhanced oil recovery efficiency of an acid-resistant polymer microspheres of anti-CO<sub>2</sub> channeling in low-permeability reservoirs. Petrol. Sci. 21 (4), 2420–2432. https://doi.org/10.1016/j.petsci.2024.02.002.
- Kang, W., Jiang, H., Yang, H., et al., 2021. Study of nano-SiO<sub>2</sub> reinforced CO<sub>2</sub> foam for anti-gas channeling with a high temperature and high salinity reservoir. J. Ind. Eng. Chem. 97, 506–514. <a href="https://doi.org/10.1016/j.jiec.2021.03.007">https://doi.org/10.1016/j.jiec.2021.03.007</a>.
   Kang, W., Shao, S., Yang, H., et al., 2019. The effect of stepwise increasing of water
- Kang, W., Shao, S., Yang, H., et al., 2019. The effect of stepwise increasing of water injection rates on enhanced oil recovery after preformed particle gel treatment. J. Petrol. Sci. Eng. 182, 106239. https://doi.org/10.1016/j.petrol.2019.106239.
- Kumar, N., Augusto Sampaio, M., Ojha, K., et al., 2022. Fundamental aspects, mechanisms and emerging possibilities of CO<sub>2</sub> miscible flooding in enhanced oil recovery: a review. Fuel 330, 125633. https://doi.org/10.1016/j.fuel.2022.125633.
- Lashari, Z.A., Yang, H., Zhu, Z., et al., 2018. Experimental research of high strength thermally stable organic composite polymer gel. J. Mol. Liq. 263, 118–124. https://doi.org/10.1016/j.molliq.2018.04.146.
- Liu, M., Ge, J., Zhang, G., et al., 2024. Preparation and temperature resistance mechanism of nanoparticle-enhanced polymer gel. Colloid Polym. Sci. 302 (7), 1097–1108. https://doi.org/10.1007/s00396-024-05253-y.
- Liu, Y., Rui, Z., Yang, T., et al., 2022. Using propanol as an additive to CO<sub>2</sub> for improving CO<sub>2</sub> utilization and storage in oil reservoirs. Appl. Energy 311, 118640. https://doi.org/10.1016/j.apenergy.2022.118640.
- Luo, X.-J., Wei, B., Gao, K., et al., 2023. Gas channeling control with an in-situ smart surfactant gel during water-alternating-CO<sub>2</sub> enhanced oil recovery. Petrol. Sci. 20 (5), 2835–2851. https://doi.org/10.1016/j.petsci.2023.03.003.
- Massarweh, O., Abushaikha, A.S., 2022. A review of recent developments in CO<sub>2</sub> mobility control in enhanced oil recovery. Petroleum 8 (3), 291–317. https://doi.org/10.1016/j.petlm.2021.05.002.
- Meharthaj, H., Srinivasan, S.M., Arockiarajan, A., 2020. Creep behavior of magnetorheological gels. Mech. Adv. Mater. Struct. 27 (13), 1031–1039. https://doi.org/10.1080/15376494.2020.1734698.
- Neto, V.J.S., Dores, F.G.L., Oliveira, P.F., et al., 2024. Evaluation of the influence of adding clay in polymeric hydrogels based on partially hydrolyzed polyacrylamide and aluminum citrate. J. Appl. Polym. Sci. 141 (9), e55019. https://doi.org/10.1002/app.55019.
- Nguele, R., Omondi, B.A., Yamasaki, S., et al., 2021. Evaluation of CO<sub>2</sub>-triggered and thermo-responsive gels for heterogeneous oil formations. Colloids Surf. A Physicochem. Eng. Asp. 622, 126688. https://doi.org/10.1016/ i.co/surfa.2021.126688.
- Pal, N., Zhang, X., Ali, M., et al., 2022. Carbon dioxide thickening: a review of technological aspects, advances and challenges for oilfield application. Fuel 315, 122947. https://doi.org/10.1016/j.fuel.2021.122947.
- Ramos, L., Banc, A., Louhichi, A., et al., 2021. Impact of the protein composition on the structure and viscoelasticity of polymer-like gluten gels. J. Phys. Condens. Matter 33 (14), 144001. https://doi.org/10.1088/1361-648X/abdf91.
- Ren, B., Duncan, I., 2019. Modeling oil saturation evolution in residual oil zones: implications for CO<sub>2</sub> EOR and sequestration. J. Petrol. Sci. Eng. 177, 528–539. https://doi.org/10.1016/j.petrol.2019.02.072.
- Sharma, T., Joshi, A., Jain, A., et al., 2022. Enhanced oil recovery and CO<sub>2</sub> sequestration potential of bi-polymer polyvinylpyrrolidone-polyvinyl alcohol. J. Petrol.

- Sci. Eng. 211, 110167. https://doi.org/10.1016/j.petrol.2022.110167.
- Song, T., Zhai, Z., Liu, J., et al., 2022. Laboratory evaluation of a novel Self-healable polymer gel for CO<sub>2</sub> leakage remediation during CO<sub>2</sub> storage and CO<sub>2</sub> flooding. Chem. Eng. J. 444, 136635. https://doi.org/10.1016/j.cej.2022.136635.
- Sun, X., Suresh, S., Zhao, X., et al., 2018. Effect of supercritical CO<sub>2</sub> on the dehydration of polyacrylamide-based super-absorbent polymer used for water management. Fuel 224, 628–636. https://doi.org/10.1016/j.fuel.2018.03.103.
- Tang, X., Zhou, B., Chen, C., et al., 2020. Regulation of polymerizable modification degree of nano-SiO<sub>2</sub> and the effects on performance of composite microsphere for conformance control. Colloids Surf. A Physicochem. Eng. Asp. 585, 124100. https://doi.org/10.1016/j.colsurfa.2019.124100.
- Wang, H., Liao, X.W., Zhao, X.L., 2014. The influence of CO<sub>2</sub> solubility in reservoir water on CO<sub>2</sub> flooding and storage of CO<sub>2</sub> injection into a water flooded low permeability reservoir. Energy Sources, Part A Recovery, Util. Environ. Eff. 36 (8), 815–821. https://doi.org/10.1080/15567036.2012.741654.
- Yang, H., Iqbal, M.W., Lashari, Z.A., et al., 2019. Experimental research on amphiphilic polymer/organic chromium gel for high salinity reservoirs. Colloids Surf. A Physicochem. Eng. Asp. 582, 123900. https://doi.org/10.1016/i.colsurfa.2019.123900.
- Yang, H., Kang, W., Tang, X., et al., 2018. Gel kinetic characteristics and creep behavior of polymer microspheres based on bulk gel. J. Dispersion Sci. Technol.

- 39 (12), 1808-1819. https://doi.org/10.1080/01932691.2018.1462192.
- Yang, H., Kang, W., Wu, H., et al., 2016. Passive microrheology for measurement of gelation behavior of a kind of polymer gel P(AM-AA-AMPS). J. Appl. Polym. Sci. 133 (17), 43364. https://doi.org/10.1002/app.43364.
- Yang, H., Lv, Z., Wang, L., et al., 2023. Stability mechanism of controlled acidresistant hydrophobic polymer nanospheres on CO<sub>2</sub> foam. Fuel 346, 128332. https://doi.org/10.1016/j.fuel.2023.128332.
- Yang, H., Xu, Z., Zhao, Y., et al., 2024. A strong stability gel foam for water shutoff during oil and gas reservoir development. Phys. Fluids 36 (2), 027133. https:// doi.org/10.1063/5.0185771.
- Zhang, S., Guo, J., Gu, Y., et al., 2020. Polyacrylamide gel formed by Cr(III) and phenolic resin for water control in high-temperature reservoirs. J. Petrol. Sci. Eng. 194, 107423. https://doi.org/10.1016/j.petrol.2020.107423.
- Zhou, B., Kang, W., Jiang, H., et al., 2022. Preparation and crosslinking mechanism of delayed swelling double-crosslinking nano polymer gel microsphere for anti-CO<sub>2</sub> gas channeling. J. Petrol. Sci. Eng. 219, 111122. https://doi.org/10.1016/ i.petrol.2022.111122.
- Zhou, B., Kang, W., Yang, H., et al., 2021. Preparation and properties of an acid-resistant preformed particle gel for conformance control. J. Petrol. Sci. Eng. 197, 107964. https://doi.org/10.1016/j.petrol.2020.107964.